Influence of growth velocity v and temperature gradient G on the interlamellar spacing λ of FeC unidirectionally crystallized eutectic

Adrian Świątkowski

adrswi@agh.edu.pl | https://orcid.org/0000-0003-3767-4749

AGH University of Krakow,

Faculty of Foundry Engineering

Reymonta 23 St. 30-059 Krakow, Poland

Tomasz Wiktor

twiktor@agh.edu.pl | https://orcid.org/0000-0002-8219-2397

AGH University of Krakow,

Faculty of Foundry Engineering

Reymonta 23 St. 30-059 Krakow, Poland

Dariusz Kopyciński

djk@agh.edu.pl | https://orcid.org/0000-0003-1651-2740

AGH University of Krakow,

Faculty of Foundry Engineering

Reymonta 23 St. 30-059 Krakow, Poland

(Received 04 August 2025; Accepted 19 May 2026)

Abstract

The paper presents results of investigations concerning the influence of the growth velocity (v) and temperature gradient (G) on the interlamellar spacing (λ) in an irregular iron-carbon (Fe-C) eutectic unidirectionally crystalized. The aim of this study was to verify the growth model of D.J. Fisher and W. Kurz and to determine the relationship λ = f(v, G) based on experimental and numerical analysis. The crystallization process was carried out using the Bridgman-Stockbarger method with liquid metal cooling (LMC), and the structure was studied using optical microscopy and scanning electron microscope. In parallel, numerical simulations were performed in ProCAST to determine the temperature gradient in the liquid at the crystallisation front. The results showed that increasing the growth velocity at constant G leads to a decrease in the interlamellar spacing λ, while at constant velocity a decrease in G results in an increase in λ. The experimental data obtained showed good agreement with the results of mathematical modelling, confirming the suitability of the W. Kurz and D.J. Fisher model in describing the crystallisation of irregular Fe-C eutectics alloys.

Keywords: Fe-C alloy, directional solidification, interlamellar spacing, growth rate, thermal gradient,

Introduction

The process of eutectic crystallization is one of the key physico-chemical phenomena occurring during phase transitions in metal alloys that fundamentally determines the structure, and thus the functional properties, of the alloys. Understanding the mechanism of eutectic crystallization enables conscious control of this process in order to achieve an optimal alloy structure. The practical importance of mastering the mechanism of eutectic crystallization is particularly important in the case of iron-carbon alloys, which are widely used in the automotive, power and engineering industries, playing a key role in the geometry of the structure and thus allowing the improvement of such properties as fatigue strength, wear resistance, machinability or thermal conductivity [1,2]. Proper design of the structure and skilful reproduction during melting directly affect the reliability and durability of castings. The process of unidirectional eutectic crystallization is carried out using specialised equipment that ensures continuous unidirectional heat dissipation. [3,4]. One method is the use of Bridgman unidirectional crystallization technology, which allows alloys with better mechanical properties to be obtained. The issue of eutectic structure formation has been the subject of numerous studies for many years in relation to volumetric and unidirectional crystallization [5,6,7,8,9]. One of the parameters describing the structure of the eutectic is the interlamellar spacing (λ), which forms the basis for assessing the homogeneity of the microstructure and the quality of the casting. Under conditions of unidirectional crystallization, process parameters such as the growth velocity of the crystallization front (v) and the temperature gradient (G) in the liquid phase are fundamental to the formation of the size and geometry of the eutectic phases [10,11]. An analysis of various model of the eutectic growth law shows that some of them take into account the relation λ=f(v), where: v - the eutectic growth velocity v, while others take into account both: the eutectic growth velocity v and the temperature gradient in the liquid at the crystallization front G, λ=f(v, G) [6].

The figure below (Fig. 1) shows a diagram of the shape of the front of irregular eutectic crystallization used in the modelling of eutectic growth by D.J. Fisher and W. Kurz:

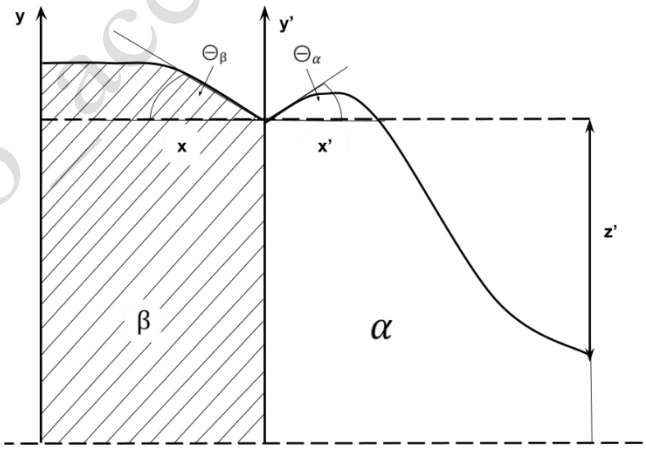

Figure 1. Schematic of the shape of the irregular eutectic crystallization front using in the modelling of eutectic growth by D.J Fisher and W. Kurz

The model of D.J Fisher and W Kurz is based on the concept of weakly coupled eutectic growth, and takes into account the influence of the temperature gradient in the liquid at the crystallization front G. A characteristic feature of graphitic eutectic growth is the phenomenon of branching of the faceted phase, which is a result of the non-traction of the crystallization front. With the movement of the crystallization front in the liquid, the local

interlamellar spacing $\lambda_1$is increased to a certain maximum value λ_2 and then the phenomenon of faceted phase branching occurs. Then the branching increases in its crystallographic direction, which is incompatible with the direction of heat flow. The increase in branching continues until the interlamellar spacing reaches λ_1 [12,13]. This phenomenon limits the average interlamellar spacing, determined by the following formula:

$$\overline{\lambda} = (\lambda_1 + \lambda_2) * \frac{1}{2} \tag{1}$$

It follows that, during the movement of an irregular eutectic crystallization front with the given velocity v, and the given temperature gradient G, there are areas charateristic of a regular eutectic structure λ_1 and a locally stable crystallization front, and areas where β-faceted phase branching is observed, λ_2 (unstable front). The kinetics of faceted phase growth depends on the mechanism of planar defects, which have been described in other work [14,15,16,17]. On the crystallization front of the non-faceted phase α, an irregular eutectic, in the region of the structure λ_2, there is a characteristic cavity z', marked in the figure above (Fig. 1.), which is described by the third degree function shown below:

$$y = ax^3 + bx^2 + cx + d \tag{2}$$

where:

x, y – coordinates (Fig. 1.),

a, b, c, d – constants.

Assuming appropriate boundary conditions, the independent constants a, b, c, d are determined, which allows the determination of the relation describing the complex shape of the front at the microscopic scale shown below:

$$y = \frac{z'}{\Psi_\alpha}\left[(2\Psi + 1) * \left(\frac{x'}{S_\alpha}\right)^3 - (3\Psi + 2) * \left(\frac{x'}{S_\alpha}\right)^2 - \left(\frac{x'}{S_\alpha}\right)\right] \tag{3}$$

in which:

$$\Psi = \frac{z'}{S_\alpha tg\Theta_\alpha} = \frac{2z'}{\lambda f_\alpha tg\Theta_\alpha} \tag{4}$$

In the final stage of the procedure, a relation is obtained that takes into account five variables: the degree of undercooling (ΔT), the interlamellar spacing (λ), the growth velocity (v), the temperature gradient (G) and the cavity (z'). Assuming a constant growth velocity (v = const) and taking into account the mean parameter ($\overline{\lambda}$), according to equation above, a numerical calculation is performed in which the cavity z' is eliminated. This allows the remaining variables to be related as shown below:

$$\frac{\lambda^2 * v}{G^{-n}} = const \tag{5}$$

where:

n – exponent, depending on the type of alloy. For Fe-C it is 0,7 [7].

Despite significant progress in the development of the theory of Fe-C eutectic growth laws and experimental and computational tools, there are still a limited number of studies combining experimental and modelling approaches. The aim of the present work is to conduct experimental and numerical studies to verify the growth model of D.J Fisher and W. Kurz for irregular Fe-C eutectics and to determine the relationship between the growth velocity v, the temperature gradient G and the interlamellar spacing λ. This work is an attempt to fill the cognitive gap regarding the influence of thermal conditions of crystallization on Fe-C microstructure.

Research methodology

The material for testing was collected under industrial conditions. Test specimens in the shape of a cylinder with a diameter of 5 mm and a height of 100 mm were melted in an induction furnace for unidirectional crystallization using the Bridgman-Stockbarger method with a vertical temperature gradient in a ceramic crucible with a wall thickness of 0.5 mm. The heating chamber of the furnace was heated to 1400° C at a rate of 75°C/min. Once the thermal conditions in the furnace chamber were stabilised, the specimens was pulled towards the cooler at a constant velocity of 9 – 40 mm/h. Temperature maintenance of the cooler is carried out with water at a temperature of approximately 22°C. In order to eliminate the gas gap between the cooler and the crucible (and to increase the temperature gradient G), it was filled with a high boiling point metal alloy which is liquid at ambient temperature (68.5 wt.% Ga, 21.5 wt.% In and 10 wt.% Zn). The special device for unidirectional crystallization technology with LMC is shown below (Fig. 2.):

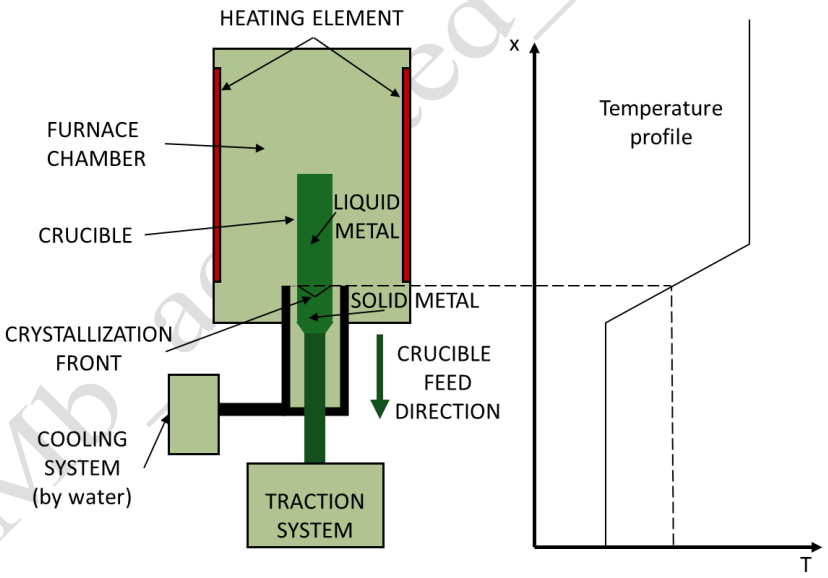

Figure 2. Diagram of a furnace for unidirectional crystallization using the Bridgman method with liquid metal cooling LMC

The research was carried out at the Department of Cast Alloys and Composites Engineering, Faculty of Foundry Engineering, AGH. The table (Tab. 1.) below shows the chemical composition of the investigated alloy. The chemical composition of the alloy was analyzed using a SpectroMaxx Emission Spectrometer.

Table 1. Analyzed chemical composition of cast iron

	C	Si	Mn	Cu	P	Mg	Cr	Ti	Ni	S	Al	Pb	Sn
Chemical composition, % mass	3,840	1,880	0,200	0,030	0,030	0,039	0,030	0,016	0,010	0,008	0,007	0,002	0,002

Qualitative and quantitative metallographic analysis was carried out on the longitudinal section of the samples using a KEYENCE VXH-7100 optical microscope connected to computer software and using a scanning electron microscope (SEM) from JEOL JSM 5500LV company. Specimens were digested in 5% nitric acid solution (HNO_3), in ethanol (C_2H_5OH) - with Nital reagent. The geometrical parameter $\bar{\lambda}$, i.e. the average interlamellar spacing, was measured in the oriented part of the eutectic as the ratio of the length of the measurement lines $\sum L$ to the number of intersections f of these lines through the graphite particles [16,18].

$$\bar{\lambda} = \frac{\sum L}{f}$$

Numerical simulations allow an accurate representation of the thermal conditions in the system and were carried out using ProCAST software [19]. The conditions present in the unidirectional crystallization device used in the research were simulated (Fig. 3).

The temperature distribution in the sample is shown below (Fig. 3.), along with the overall system:

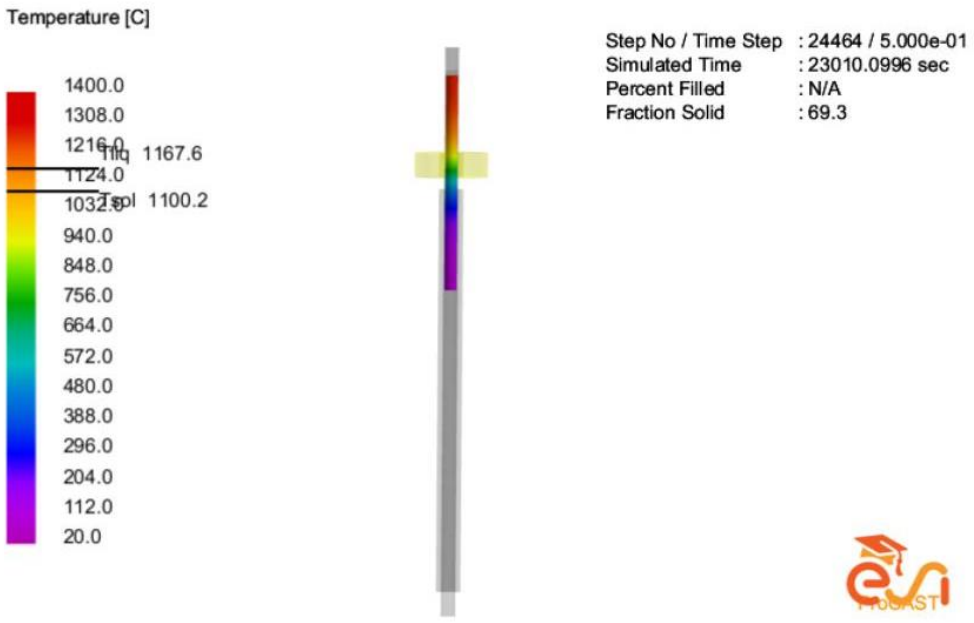

Figure 3. Simulation in ProCAST software - temperature distribution in the sample with the whole system, growth rate $v = 2{,}50 * 10^{-6}\ m/s$ (liquidus temperature 1167,6°C, solidus temperature 1100,2°C)

The liquidus and solidus temperatures in ProCAST are calculated based on the CALPHAD thermodynamic databases, the chemical composition of the alloy, and the solidification model (Lever). The amount of solid phase changes non-linearly and depends on the chemical

composition and solidification conditions (the physicochemical state of the liquid metal). At the liquidus temperature, the entire metal is liquid, where as at the solidus temperature, it is solid.

ProCAST software was also used to determine the temperature gradient in the liquid at the crystallization front. The profile from the beginning to the end of the specimen was determined (Fig. 5). Then, the furnace feed was simulated at a given velocity and the temperature of the liquid metal was recorded along the route of its movement (Fig. 4.), i.e. the function $T(x)$; where x is the distance from the beginning of the specimen. After numerical differentiation of the curve of the function $T(x)$, the curve $\frac{dT}{dx}$, i.e. the distribution of the temperature gradient in the alloy G, was obtained (Fig. 7). The data were narrowed down to the range between the liquidus temperature T_L and the solidus temperature T_S of the investigated alloy and then the temperature gradient in the liquid at the front of crystallization, i.e. at the liquidus temperature, was determined.

Below (Fig. 4.) is shown a plot of the temperature dependence on the profile distance and (Fig. 5.) shows the temperature distribution in the sample with the marked profile for determining the temperature gradient in the liquid at the crystallization front:

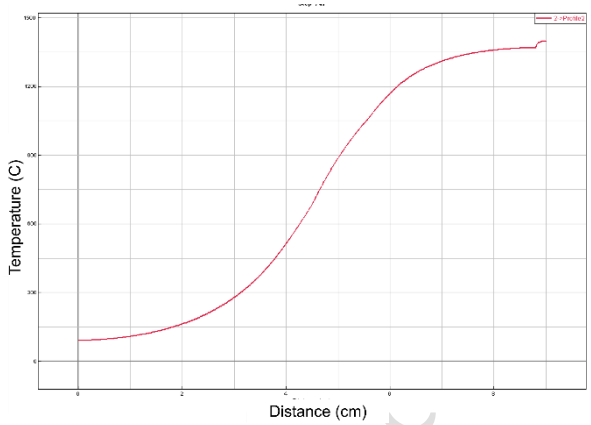

Figure 4. Plot of temperature dependence on profile distance generated in ProCAST software

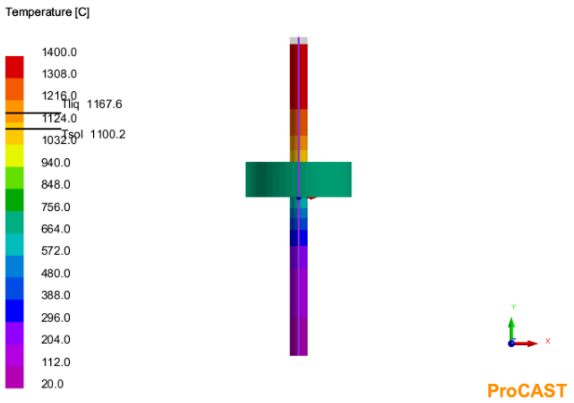

Figure 5. Simulation in ProCAST - temperature distribution in the specimen with marked profile for determining the temperature gradient, growth velocity $v = 2{,}50 * 10^{-6}\ m/s$

Below (Fig. 6.) are the results of a simulation carried out in ProCAST of the amount of solidified phase in order to visualise the crystallization front for the investigated velocities v:

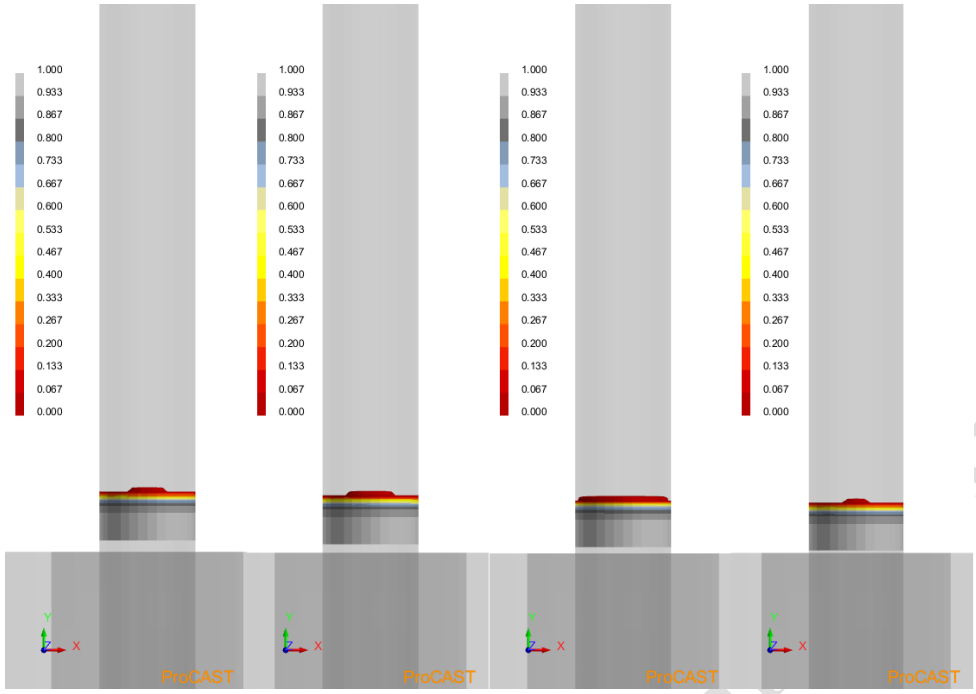

Figure 6. Simulation in ProCAST program - amount of solidified phase (crystallization front) a) $v = 2{,}50 * 10^{-6}\ m/s$*; b)* $v = 5{,}56 * 10^{-6}\ m/s$*; c)* $v = 8{,}33 * 10^{-6}\ m/s$*; d)* $v = 1{,}11 * 10^{-5}\ m/s$

The simulation shows that, independent of the growth rate, the crystallization front is correctly located above the cooler in the device for unidirectional crystallization using the Bridgman method.

Research results

Below (Fig. 7.) is a diagram showing the dependence of the temperature distribution and its gradient on the distance of the beginning of the determined profile:

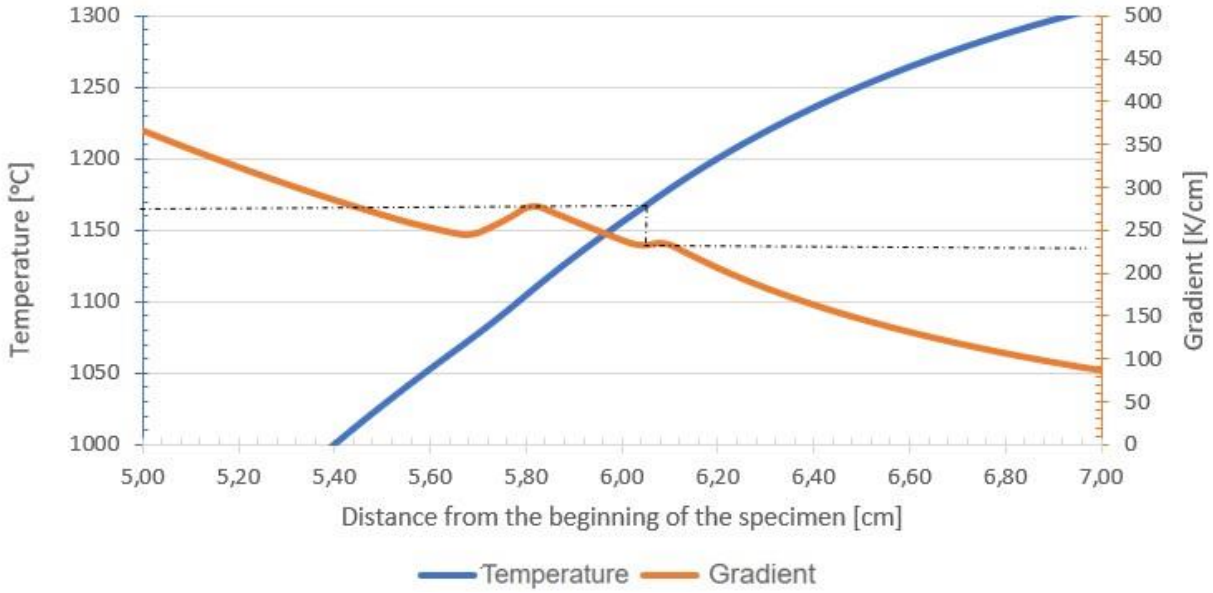

Figure 7. Plot of the temperature distribution and its gradient depending on the distance of the beginning of the profile determined in the ProCAST software

Based on the simulation results in ProCAST software and the temperature distribution in the specimen, the temperature gradient in the liquid at the crystallization front was determined. For the calculations, the gradient at temperature T_L of the investigated alloy was taken and is G = 233 [K/cm]. The obtained temperature gradient value correlates with the conditions used in the tests on the alloy at the crystallization front.

Below (Fig. 8-11.), the oriented microstrutures for different velocities are shown together with the marked direction of eutectic growth.

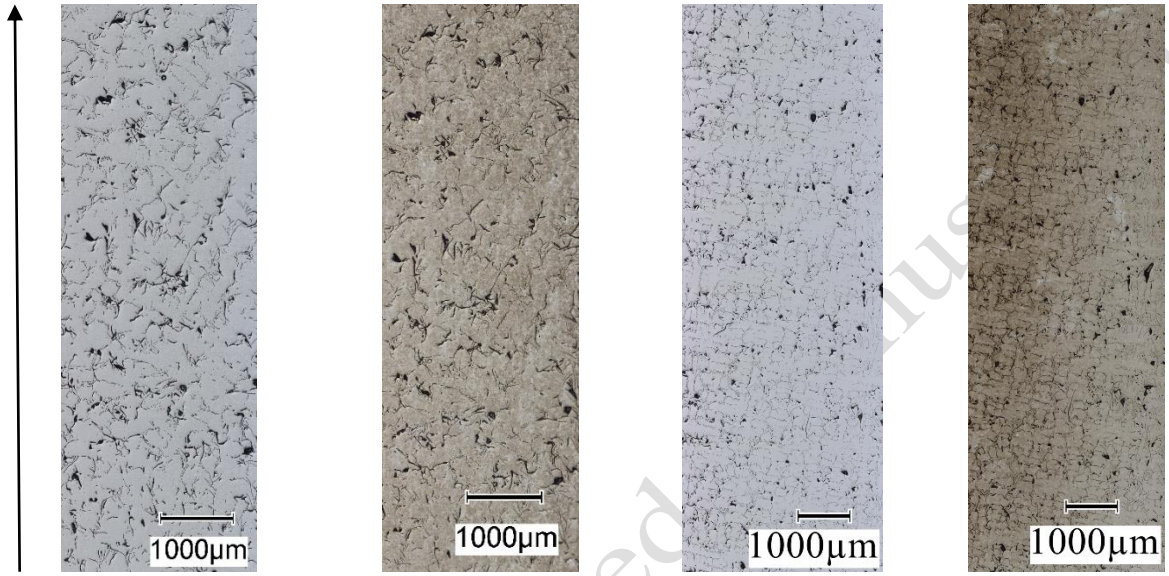

Figure 8. Unidirectional structure, growth velocity $v = 2{,}50 * 10^{-6}\ m/s$, on the right, etched with Nital

Figure 9. Unidirectional structure, growth velocity $v = 5{,}56 * 10^{-6}\ m/s$, on the right, etched with Nital

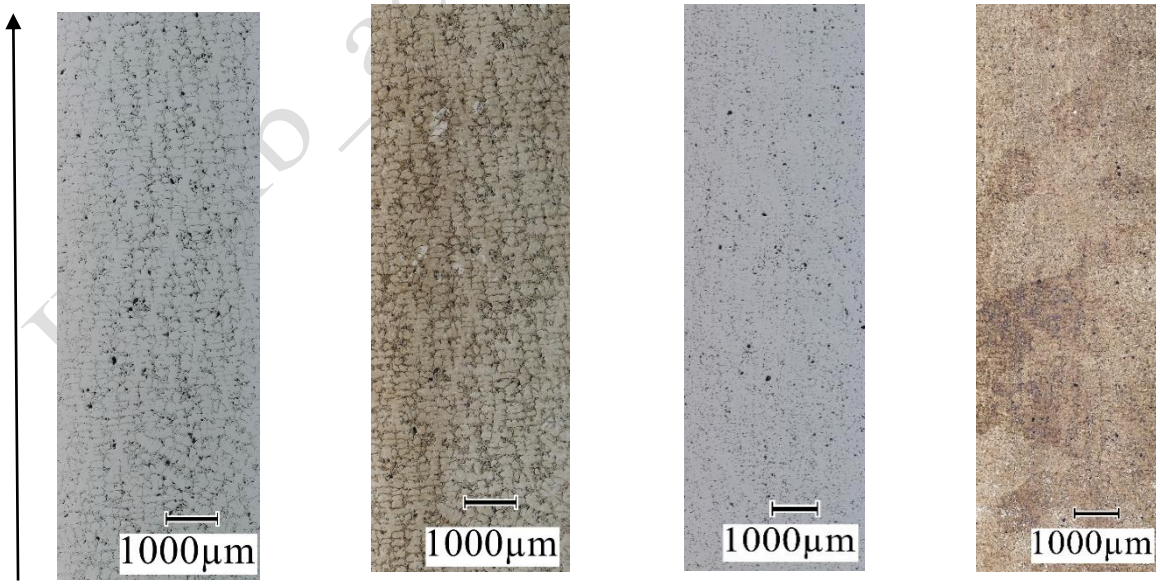

Figure 10. Unidirectional structure, growth velocity $v = 8{,}33 * 10^{-6}\ m/s$, on the right, etched with Nital

Figure 11. Unidirectional structure, growth velocity $v = 1{,}11 * 10^{-5}\ m/s$, on the right, etched with Nital

As the growth velocity increases, the interlamellar spacing decrease. The matrix is pearlitic and it does not change with increasing growth velocity for the alloy studied. Selected locations of the unidirectional microstrutures for the tested velocities are shown below (Fig. 12.):

a)

b)

c)

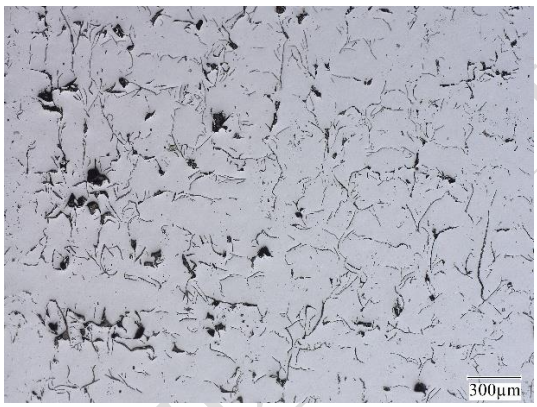

d)

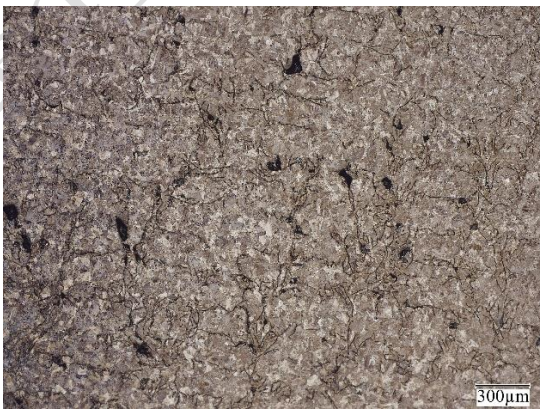

e)

f)

g) h)

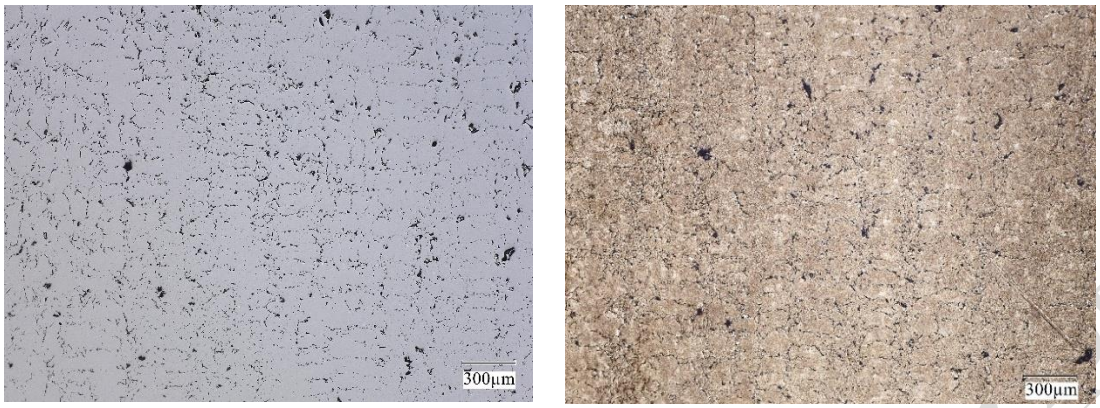

Figure 12. Unidirectional structure, a) $v = 2{,}50 * 10^{-6}\ m/s$; b) $v = 2{,}50 * 10^{-6}\ m/s$, etched with Nital; c) $v = 5{,}56 * 10^{-6}\ m/s$; d) $v = 5{,}56 * 10^{-6}\ m/s$, etched with Nital; e) $v = 8{,}33 * 10^{-6}\ m/s$; f) $v = 8{,}33 * 10^{-6}\ m/s$, etched with Nital; g) $v = 1{,}11 * 10^{-5}\ m/s$; h) $v = 1{,}11 * 10^{-5}\ m/s$, etched with Nital

Selected images of microstructures obtained by SEM are shown below (Fig. 13.):

a) b)

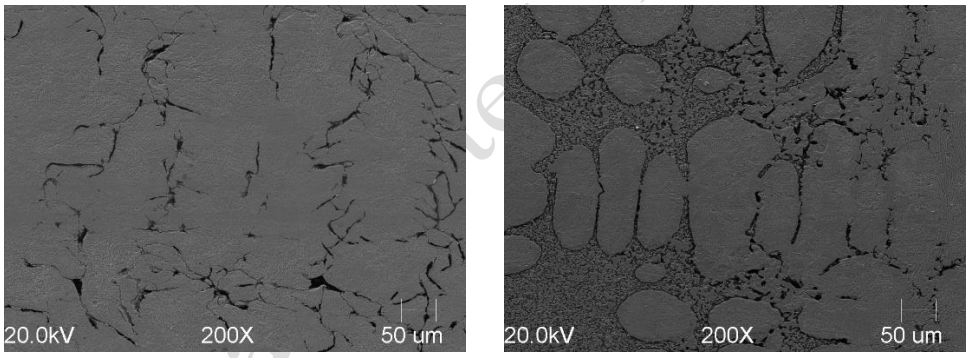

Figure 13. Microstructure images obtained using scanning electron microscopy $v = 1{,}11 * 10^{-5}\ m/s$, a) unidirectional structure, b) structure of the crystallization front

Below (Fig. 14.) are maps showing the distribution of selected elements for the selected specimen and crystallization growth velocity of v = $1{,}11 * 10^{-5}$ m/s:

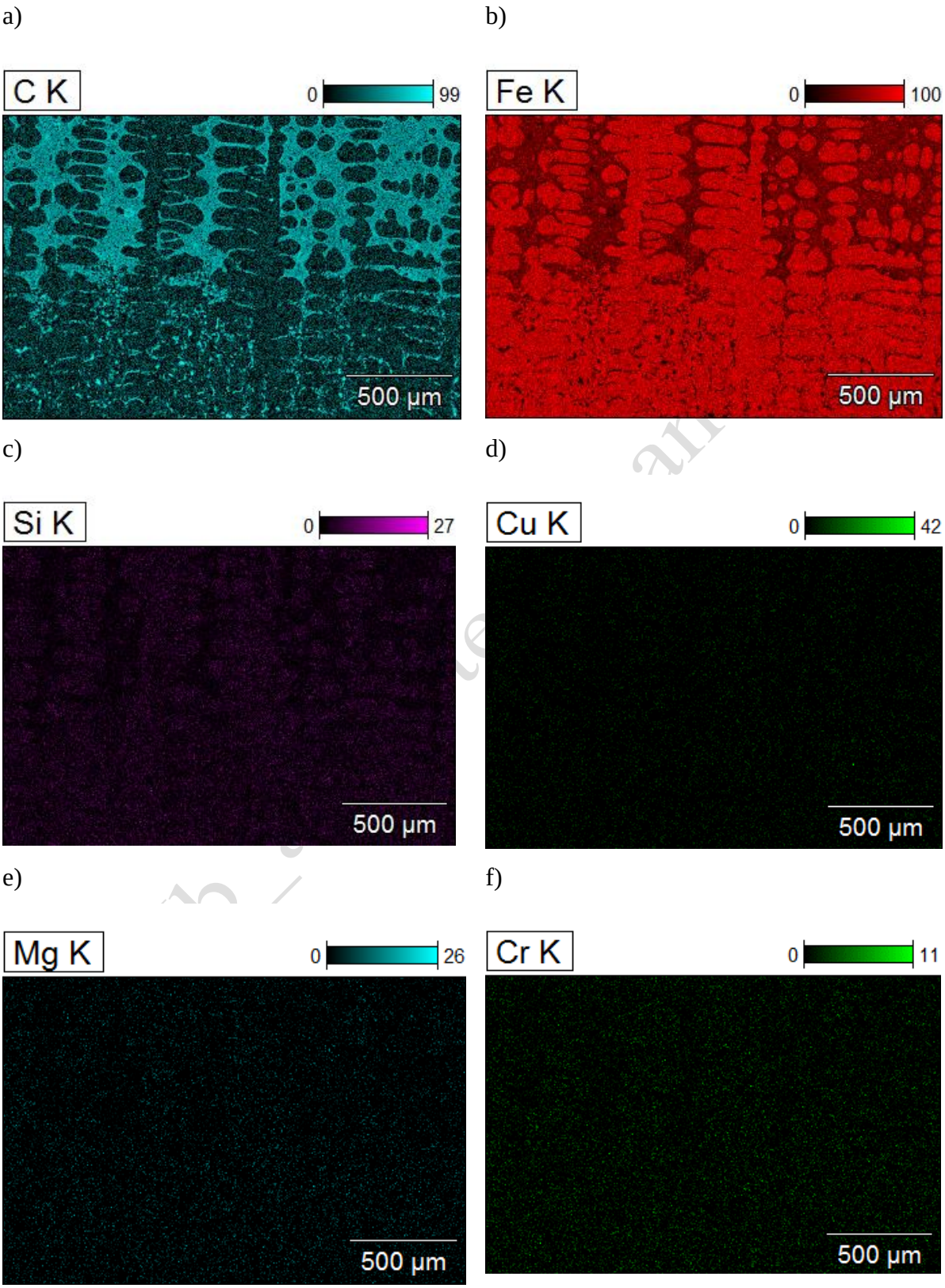

Figure 14. Element distribution maps; a) C, b) Fe, c) Si, d) Cu, e) Mg, f) Cr; Acc. Volgate. 20.0 kV, magnification 200x, Detector: EDS

The table below (Tab. 2.) shows the results of the interlamellar spacing λ investigated experimentally and calculated from the model of D. J. Fisher and W. Kurz for different velocities v, and different temperature gradient G:

Table 2. Test results of the interlamellar spacing λ [m]

Growth velocity, v [m/s]		$1{,}11 * 10^{-5}$	$8{,}33 * 10^{-6}$	$5{,}56 * 10^{-6}$	$2{,}50 * 10^{-6}$
interlamellar spacing, λ [m] – determined experimentally	G = 233 [K/cm]	$6{,}22 * 10^{-5}$ $\pm 0{,}79 * 10^{-5}$	$7{,}86 * 10^{-5}$ $\pm\ 0{,}86 * 10^{-5}$	$1{,}03 * 10^{-4}$ $\pm 0{,}069 * 10^{-4}$	$1{,}46 * 10^{-4}$ $\pm 0{,}16 * 10^{-4}$
interlamellar spacing, λ [m] – D.J. Fisher and W. Kurtz model	G = 150 [K/cm]	$7{,}26 * 10^{-5}$	$9{,}16 * 10^{-5}$	$1{,}20 * 10^{-4}$	$1{,}70 * 10^{-4}$
	G = 100 [K/cm]	$8{,}36 * 10^{-5}$	$1{,}06 * 10^{-4}$	$1{,}38 * 10^{-4}$	$1{,}96 * 10^{-4}$
	G = 50 [K/cm]	$1{,}07* 10^{-4}$	$1{,}35 * 10^{-4}$	$1{,}76 * 10^{-4}$	$2{,}5 * 10^{-4}$

The plot below (Fig. 15.) shows the dependence $\lambda = f(v)$ for the experimental results and those calculated according to the D.J Fischer and W. Kurtz model and the different temperature gradients $50 < G < 150$ $[K/cm]$, together with the marked trend lines:

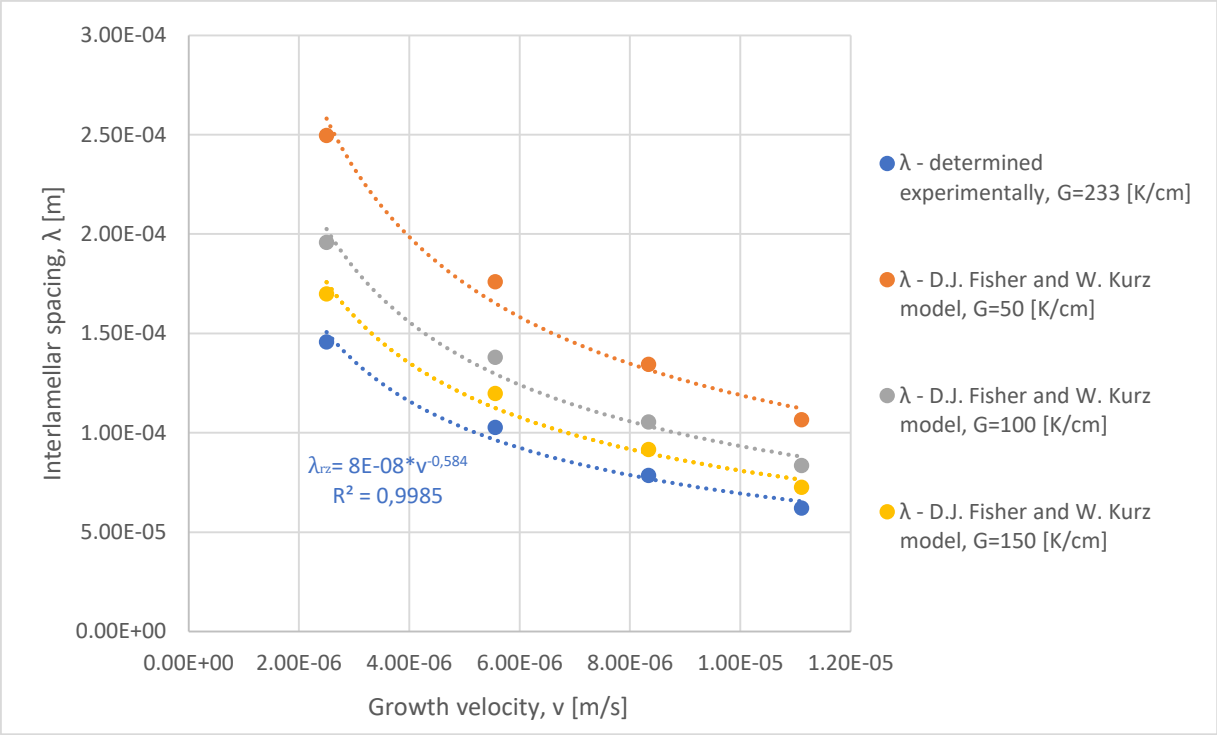

Figure 15. Dependence diagram $\lambda = f(v)$; λ - interplate distance, v - eutectic growth rate

The experimental results of the dependence $\lambda = f(v)$, for temperature gradient $G = 233\ K/cm$, were worked out statistically, obtaining the regression equation in the form of $\lambda = 8 * 10^{-8} * v^{-0584}$ and the correlation coefficient $R^2 = 0{,}9985$. The influence of the temperature gradient G in the model by D.J. Fisher and W. Kurz on the interlamellar spacing, λ was also investigated, and its influence on the interplate distance was demonstrated.

Conclusions

Research was carried out on the interlamellar spacing, λ in the dependence of crystallization parameters such as solidification velocity v and temperature gradient G for the Fe-C irregular eutectic was carried out, and the relationship between them was obtained by statistical analysis. The tests carried out allowed the relationship of the eutectic growth law $\lambda = 8 * 10^{-8} * v^{-0{,}584}$ to be established for the alloy studied. The analysis of the test results shows that, at a constant temperature gradient G, an increase in the growth velocity v results in a decrease in the interlamellar spacing λ. Above, the analysis of the test results shows that, at constant velocity v, a decrease in the temperature gradient G results in an increase in the interlamellar spacing λ.

Acknowledgments

The research was carried out at the Department of Cast Alloys and Composites Engineering, Faculty of Foundry Engineering, AGH.

Conflict of interest

The authors declare that there is no conflict of interest.

References

1. D.M. Stefanescu, Science and Engineering of Casting Solidification, Springer Cham, 2009, p.379-434.
2. C.R. Loper, R.B. Gundlach, D.M. Stefanescu, Solidification Characteristics of Cast Irons, American Foundry Society Transactions, v.96, 1988, p.761–768.
3. E. Fraś, Krystalizacja metali i stopów (Crystallization of metals and alloys), PWN, Warszawa, 1992, (in Polish).
4. E. Fraś, Directional crystallization of graphite eutectic, Zeszyt naukowy AGH, Metalurgia Odlewnictwa, v.2 (1) (1976), p. 103.
5. K.A. Jackson, J.D. Hunt, Lamellar and rod eutectic growth, Transactions of the Metallurgical Society of AIME, v.236, (1966) , p.1129–1142. https://doi.org/10.1016/B978-0-08-092523-3.50040-X
6. D.J. Fisher, W. Kurz, A teory of branching limited growth of irregular eutectitcs, Acta Metallurgical, v. 28 (6) (1980), p. 777-794. https://doi.org/10.1016/00016160(80)90155-8
7. E. Guzik, A model of irregular eutectic growth taking as an example the graphite eutectic in Fe-C alloys, Dissertations Monographies 15, AGH, Kraków, 1994
8. E. Guzik, D. Kopyciński, Modelling structure parameters of irregular eutectic growth: Modification of Magnin-Kurz theory, Metallurgical and Materials Transactions, (2006), p. 3057-3067. https://doi.org/10.1007/s11661-006-0187-7
9. E. Fraś, Krystalizacja żeliwa (Crystallization of cast iron), skrypt AGH, Kraków, 1981 (in Polish)
10. M. Trepczyńska-Łent, Possibilities of the Materials Properties Improvement for the Cementite Eutectic by Means of Unidirectional Solidification, Archives of Metallurgy and Materials, v.58 (3) (2013), p. 987-991. https://doi.org/10.2478/amm-2013-0116
11. M. Trepczyńska-Łent, Characteristics of the growth of the directionally solidified Fe-4,25% C eutectic alloy, Archives of Metallurgy and Materials, v. 66 (4) (2021), p. 1179-1186. https://doi.org/10.24425/ams.2021.138601
12. W. Kurz, D.J. Fisher, Dendrite growth at the limit of stability: tip radius and spacing, Acta Metallurgica, v. 29 (1) (1981), p. 11–20. https://doi.org/10.1016/0001-6160(81)90082-1
13. W. Wołczyński, Pattern selection in the eutectic growth – thermodynamic interpretation, Archives of Metallurgy and Materials, v. 65 (2) (2020), p. 653-666. https://doi.org/10.24425/amm.2020.132804
14. E. Fraś, Teoretyczne podstawy krystalizacji. Część II. (Theoretical foundations of crystallization. Part II), Skrypt AGH nr 1020, Kraków, 1986. (In Polish)
15. W. Wołczynski, Concentration Micro-Field for Lamellar Eutectic Growth, Defect and Diffusion Forum, v. 272 (2007), p. 123-138. https://doi.org/10.4028/www.scientific.net/DDF.272.123

16. C. Podrzucki, Żeliwo. Struktura, właściwości, zastosowanie (Cast iron. Structure, properties, applications), ZG Stop, Kraków, 1991 (In Polish)
17. Z. Hong-bo, Ai. Xin-gang, Ch. Ming, G. Rui, Ch. Qing-song, H. Zhong-linn, Phase-field simulation study of dendritic growth in directional solidification of Fe-C alloy under varied initial solute concentrations, Material Research Express, v. 12 (2) (2025), https://doi.org/10.1088/2053-1591/adb3f6
18. S. Charnnarong, S. Harnsopa, Influence of Component Proportions in Casting Process on Hardness and the Quality of Cast Iron, Archives of Foundry Engineering, v. 23 (2) (2023), p. 35-42. https://doi.org/10.24425/afe.2023.144293
19. D. Szeliga, K. Kubiak, G. Jarczyk, The Influence of the Radiation Baffle on Predicted Temperature Gradient in Single Crystal CMSX-4 Castings, International Journal of Metalcasting, v.7 (3) (2013), p. 17-23. https://doi.org/10.1007/BF03355555

List of figure:

List of tables: